

Supplementary Information for "Dry biases in land water storage and excessive soil moisture limitation in CMIP6 models"

Francesco Giardina¹, Ryan S. Padrón^{1,2}, Benjamin D. Stocker^{3,4}, Dominik L. Schumacher¹, Sonia I. Seneviratne¹

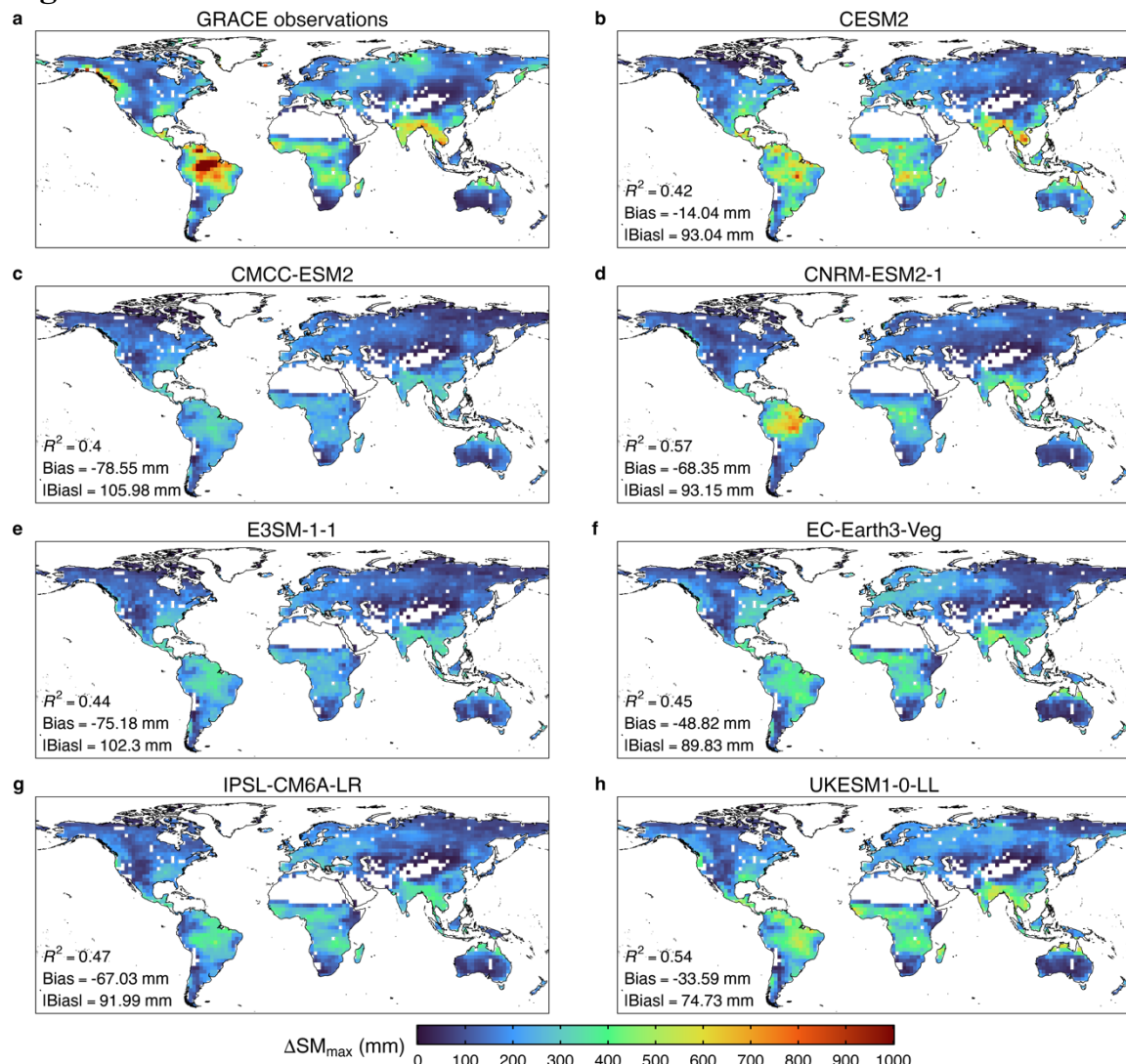
Tables

Supplementary Table 1 | CMIP6 model information

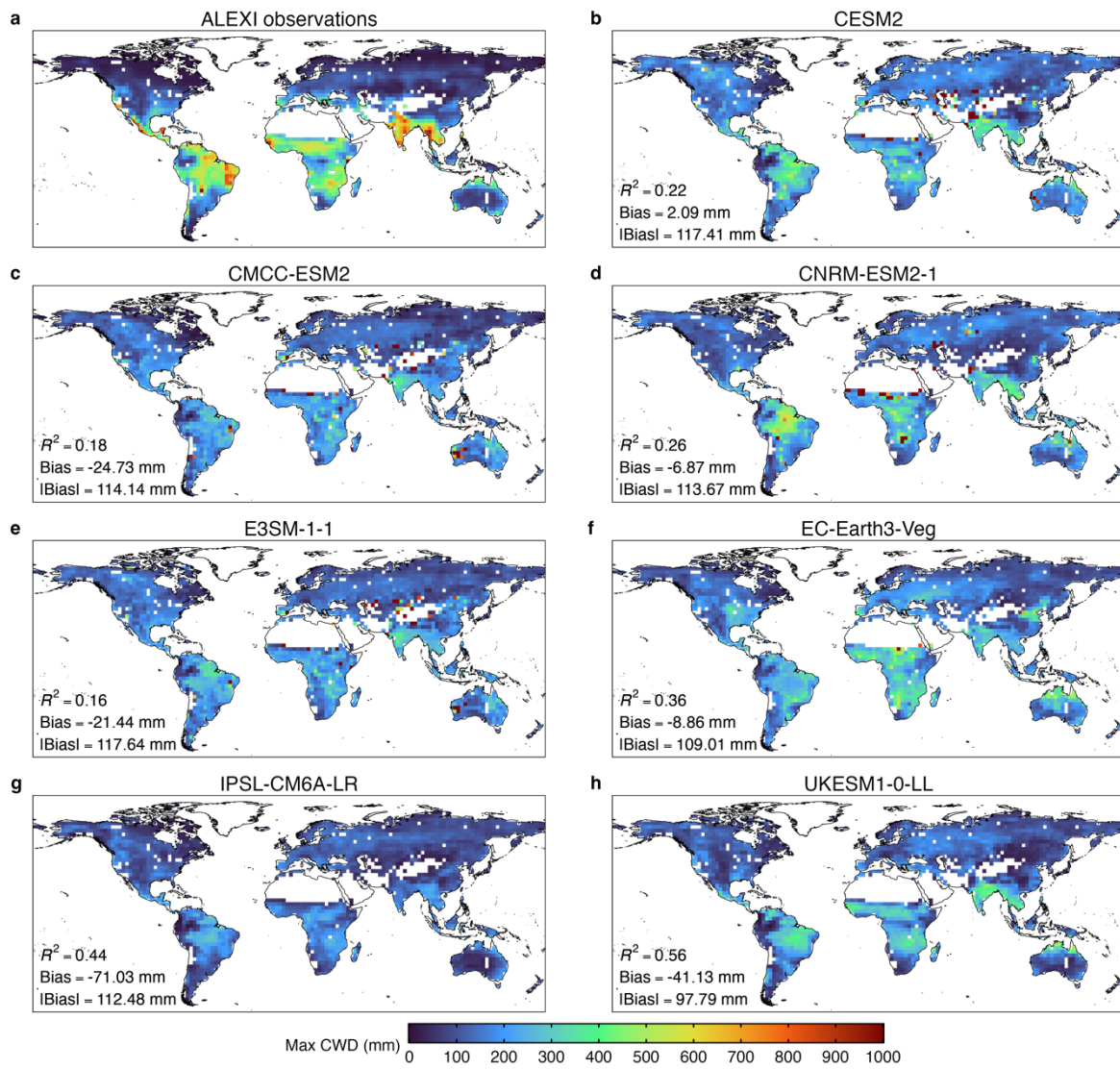
ESM Acronym	Hist/Land-Hist Run ID	References	Notes
CESM2	r1i1p1f1	Kennedy et al. [2019] ¹ Lawrence et al. [2019] ²	<ul style="list-style-type: none"> representation of LAI dynamics (LAI seasonality is not constant) representation of water stress based on leaf water potential
CMCC-ESM2	r1i1p1f1	Cherchi et al. [2019] ³	<ul style="list-style-type: none"> interactive land surface model no representation of vegetation properties interactive terrestrial carbon-cycle processes
CNRM-ESM2-1	r1i1p1f2	Séférian et al. [2019] ⁴	<ul style="list-style-type: none"> representation of LAI dynamics (LAI seasonality is not constant) interactive land surface model interactive vegetation properties interactive terrestrial carbon-cycle processes
E3SM-1-1	r1i1p1f1	Leung et al. [2020] ⁵	<ul style="list-style-type: none"> not sure (see reference)
EC-Earth3-Veg	r1i1p1f1	Döscher et al. [2022] ⁶	<ul style="list-style-type: none"> interactive land surface model interactive vegetation properties interactive terrestrial carbon-cycle processes
IPSL-CM6A-LR	r1i1p1f1	Boucher et al. [2020] ⁷	<ul style="list-style-type: none"> representation of LAI dynamics (LAI seasonality is not constant) interactive land surface model interactive vegetation properties interactive terrestrial carbon-cycle processes
UKESM1-0-LL	r1i1p1f2	Sellar et al. [2020] ⁸	<ul style="list-style-type: none"> representation of LAI dynamics (LAI seasonality is not constant) land use change in dynamic vegetation simulations interactive vegetation cover

Table partially adapted from Ref⁹

Figures

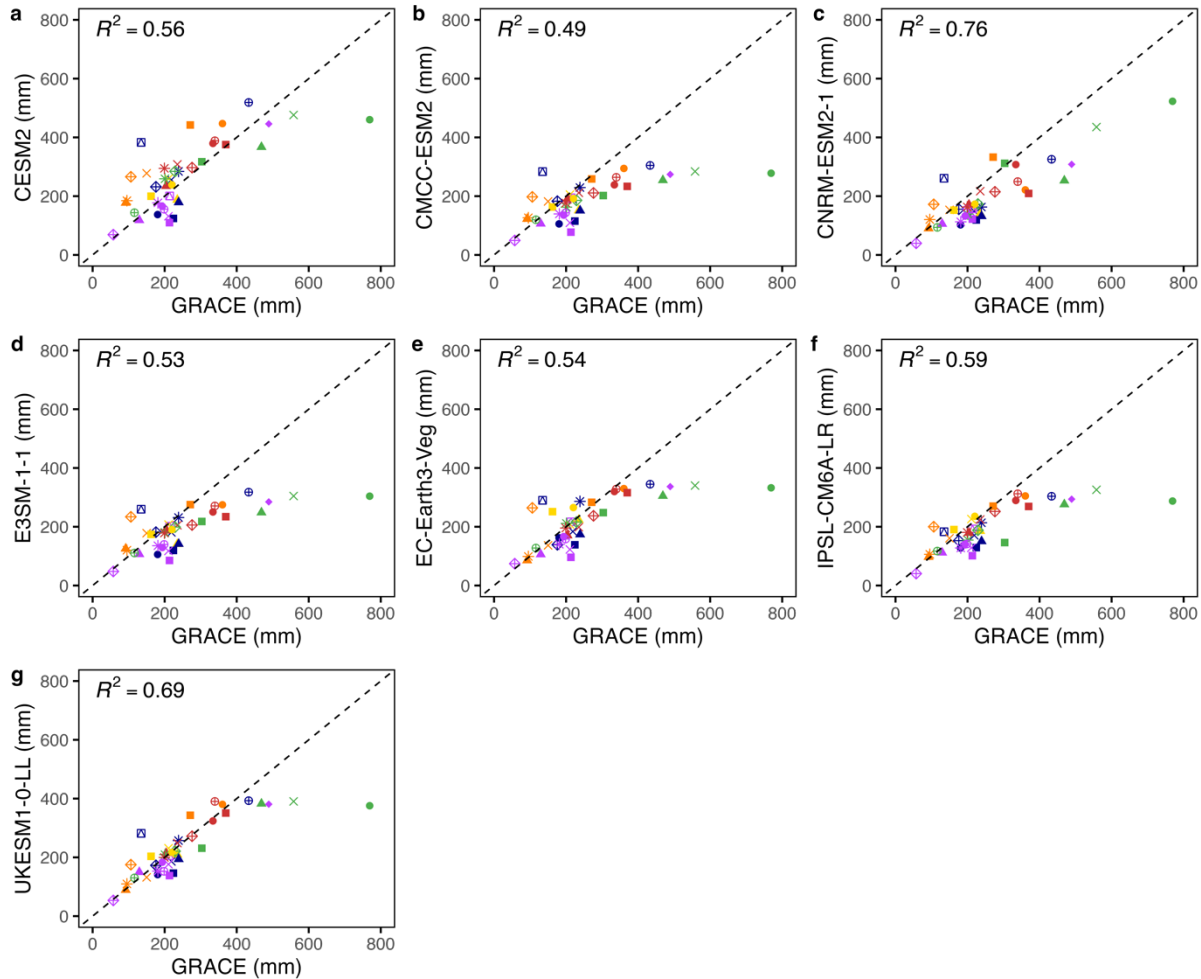


Supplementary Fig. 1 | Comparison of maximum soil moisture depletion (ΔSM_{max}) between GRACE observations and CMIP6-LMIP simulations. ΔSM_{max} was first derived for every year during 2003-2014. The maximum yearly reduction across those years was retained. **a**, ΔTWS_{max} from GRACE. **b-h**, ΔSM_{max} from CMIP6. The *land-hist* simulation was used across CMIP6 models. Bilinear interpolation was applied to harmonize the GRACE resolution with that of CMIP6. The raw bias was determined by subtracting pixel-by-pixel the observed value from each model and then calculating the mean of these differences across all pixels. For the absolute bias, we computed the mean after taking the absolute value of each pixel-wise subtraction. Values exceeding 1000 mm colored as 1000 mm for clarity.



Supplementary Fig. 2 | Maximum cumulative water deficit (CWD_{max}) derived from ALEXI observations and CMIP6 models. **A**, Maximum CWD determined from ALEXI observations, augmented using an extreme value distribution with an 80-year return period, as detailed in Ref¹⁰. **b-h**, Maximum CWD assessed over the 80 years of CMIP6 data (1935–2014), to align with the methodology used for ALEXI data. Values exceeding 1000 mm are colored as 1000 mm clarity.

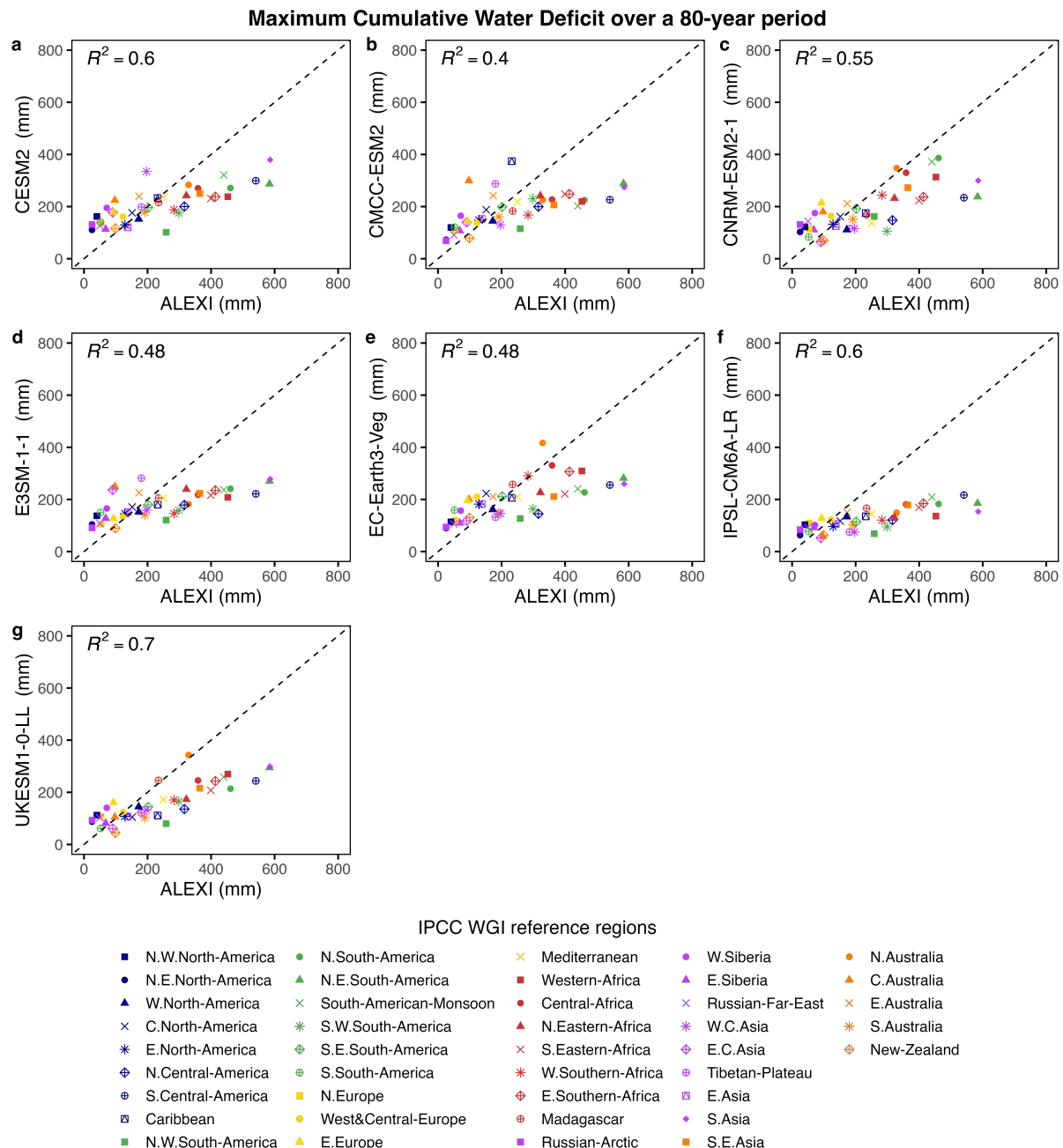
ΔSM_{max} : maximum depletion of total-column soil moisture



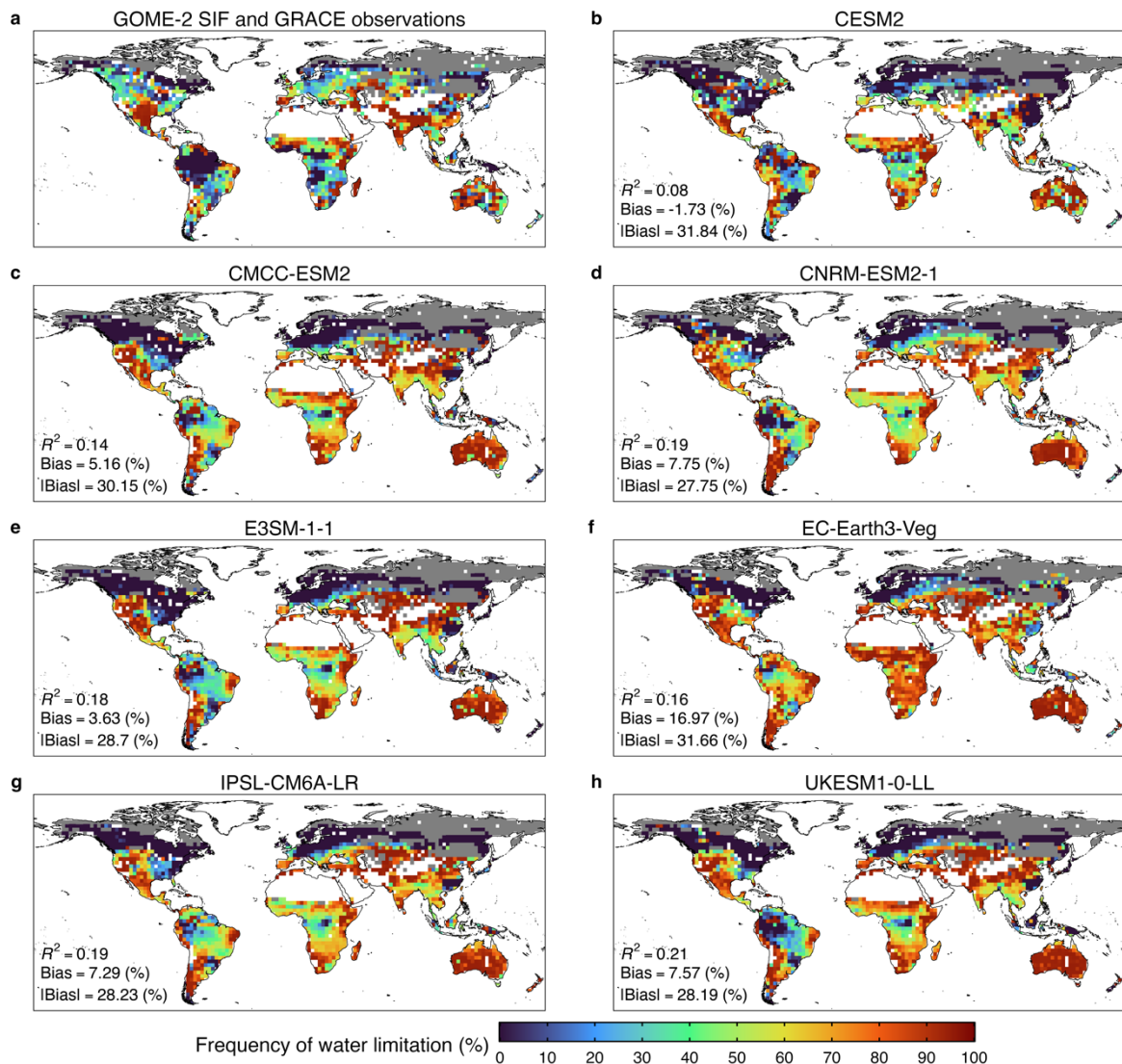
IPCC WGI reference regions

- | | | | | | | | | | | | | | | | | | | | | | | | | | | | | | | | | | | | | | | |
|---------------------|---------------------|-------------------|-------------------|-------------------|---------------------|---------------------|-------------|---------------------|-------------------|---------------------|--------------------------|---------------------|---------------------|-------------------|------------|-----------------------|--------------|------------------|-----------------|------------------|------------------|--------------------|--------------------|---------------------|---------------------|--------------|-------------|-------------|--------------------|------------|------------|------------|-------------------|---------------|---------------|---------------|---------------|---------------|
| ■ N.W.North-America | ● N.E.North-America | ▲ W.North-America | × C.North-America | * E.North-America | ◊ N.Central-America | ⊕ S.Central-America | ▢ Caribbean | ■ N.W.South-America | ● N.South-America | ▲ N.E.South-America | × South-American-Monsoon | * S.W.South-America | ◊ S.E.South-America | ⊕ S.South-America | ▢ N.Europe | ● West&Central-Europe | ○ Madagascar | ■ Russian-Arctic | ● Mediterranean | ■ Western-Africa | ● Central-Africa | ▲ N.Eastern-Africa | × S.Eastern-Africa | * W.Southern-Africa | ◊ E.Southern-Africa | ⊕ Madagascar | ▢ W.Siberia | ● E.Siberia | ▲ Russian-Far-East | × W.C.Asia | * E.C.Asia | ◊ E.C.Asia | ⊕ Tibetan-Plateau | ▢ N.Australia | ● C.Australia | × E.Australia | * S.Australia | ◊ New-Zealand |
|---------------------|---------------------|-------------------|-------------------|-------------------|---------------------|---------------------|-------------|---------------------|-------------------|---------------------|--------------------------|---------------------|---------------------|-------------------|------------|-----------------------|--------------|------------------|-----------------|------------------|------------------|--------------------|--------------------|---------------------|---------------------|--------------|-------------|-------------|--------------------|------------|------------|------------|-------------------|---------------|---------------|---------------|---------------|---------------|

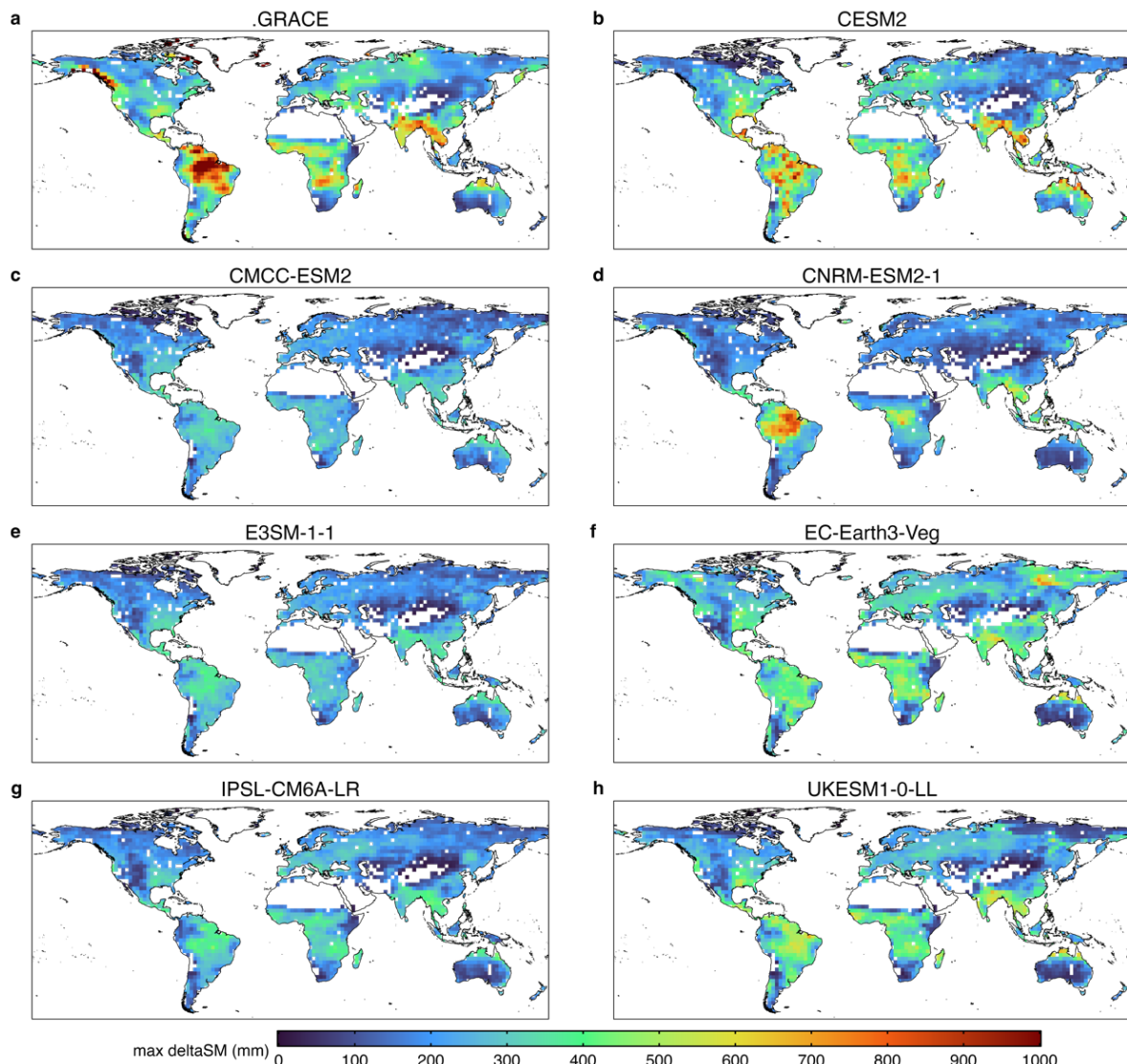
Supplementary Fig. 3 | Comparative analysis of maximum soil moisture depletion across different IPCC regions based on LMIP-CMIP6 model simulations and observations. We present a region-wise evaluation of maximum soil moisture depletion, using GRACE data and corresponding LMIP-CMIP6 model simulations. We first determined the maximum soil moisture depletion in every pixel and then we calculated the mean of this value within each IPCC region for model and observational data.



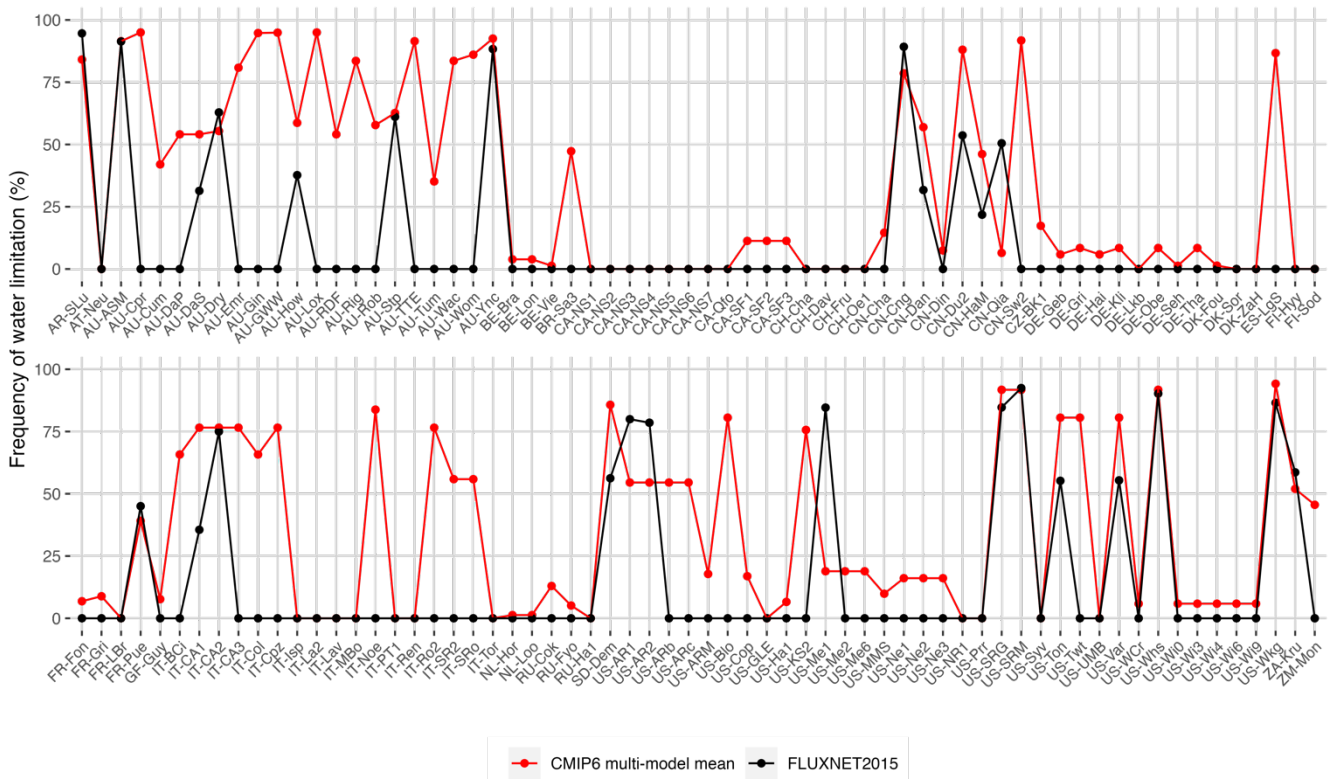
Supplementary Fig. 4 | Comparative analysis of maximum soil moisture depletion across different IPCC regions based on LMIP-CMIP6 model simulations and observations. We present a region-wise evaluation of maximum soil moisture depletion, using ALEXI data and corresponding LMIP-CMIP6 model simulations. We first determined the maximum cumulative water deficit in every pixel and then we calculated the mean of this value within each IPCC region for model and observational data.



Supplementary Fig. 5 | Global maps of frequency of soil moisture limitation. Pixel-specific critical soil moisture thresholds were first calculated to determine when plant water stress occurs. We then show the fraction of months with soil moisture below the critical threshold. **a**, Soil moisture thresholds determined with the normalized observational solar-induced fluorescence (SIF; a proxy for photosynthesis) versus normalized total water storage (TWS; the sum of soil moisture and groundwater, surface water, snow and ice) from the Gravity Recovery and Climate Experiment (GRACE, 2007-2014). **b-h**, Soil moisture thresholds calculated with the evaporative fraction (EF) vs normalized total column soil moisture with CMIP6 LMIP data (2007-2014). Dark blue pixels represent areas where no threshold could be determined by our algorithm, i.e. soil moisture is rarely limiting. On the other hand, dark red pixels represent areas that are almost always water limited. The raw bias was determined by subtracting pixel-by-pixel the observed value from each model and then calculating the mean of these differences across all pixels. Grey areas illustrate regions where the segmented regression could not be applied due to the scarcity of data points. For the absolute bias, we computed the mean after taking the absolute value of each pixel-wise subtraction. Details of all datasets and normalizations can be found in the Methods.



Supplementary Fig. 7 | Comparison of maximum soil moisture depletion (ΔSM_{max}) between GRACE observations and CMIP6 LMIP simulations. ΔSM_{max} was directly calculated over the entire time period 2003–2014. **a**, ΔSM_{max} from GRACE. **b–h**, ΔSM_{max} from CMIP6. The *land-hist* simulation was used across CMIP6 models. Bilinear interpolation was applied to harmonize the GRACE resolution with that of CMIP6. The mean bias was calculated by first computing the bias between model data and GRACE at every pixel, and then calculating the mean of all biases for the entire globe. Values exceeding 1000 mm colored as 1000 mm to address outliers.



Supplementary Fig. 8 | Frequency of soil moisture limitation at FLUXNET2015 sites. The red dotted line indicates CMIP6 multi-model mean, whereas the black dotted line indicates FLUXNET2015 data points. The multi-model mean was calculated from models UKESM1-0-LL, IPSL-CM6A-LR, EC-Earth3-Veg, and CNRM-ESM2-1, which were the only models in our selection providing daily data of the relevant variables (see Methods).

References

1. Kennedy, D. *et al.* Implementing Plant Hydraulics in the Community Land Model, Version 5. *J Adv Model Earth Syst* **11**, 485–513 (2019).
2. Lawrence, D. M. *et al.* The Community Land Model Version 5: Description of New Features, Benchmarking, and Impact of Forcing Uncertainty. *J Adv Model Earth Syst* **11**, 4245–4287 (2019).
3. Cherchi, A. *et al.* Global Mean Climate and Main Patterns of Variability in the CMCC-CM2 Coupled Model. *J Adv Model Earth Syst* **11**, 185–209 (2019).
4. Séférian, R. *et al.* Evaluation of CNRM Earth System Model, CNRM-ESM2-1: Role of Earth System Processes in Present-Day and Future Climate. *J Adv Model Earth Syst* **11**, 4182–4227 (2019).
5. Leung, L. R., Bader, D. C., Taylor, M. A. & McCoy, R. B. An Introduction to the E3SM Special Collection: Goals, Science Drivers, Development, and Analysis. *J Adv Model Earth Syst* **12**, e2019MS001821 (2020).
6. Döscher, R. *et al.* The EC-Earth3 Earth system model for the Coupled Model Intercomparison Project 6. *Geosci Model Dev* **15**, 2973–3020 (2022).
7. Boucher, O. *et al.* Presentation and Evaluation of the IPSL-CM6A-LR Climate Model. *J Adv Model Earth Syst* **12**, e2019MS002010 (2020).
8. Sellar, A. A. *et al.* Implementation of U.K. Earth System Models for CMIP6. *J Adv Model Earth Syst* **12**, e2019MS001946 (2020).
9. Brands, S. A circulation-based performance atlas of the CMIP5 and 6 models for regional climate studies in the Northern Hemisphere mid-to-high latitudes. *Geosci Model Dev* **15**, 1375–1411 (2022).
10. Stocker, B. D. *et al.* Global patterns of water storage in the rooting zones of vegetation. *Nat Geosci* **16**, 250–256 (2023).